In-*vitro* and in-*vivo* degradation studies of freeze gelated porous chitosan composite scaffolds for tissue engineering applications

Saad B. Qasim [a], Shehriar Husain [a], Ying Huang [a], Maksym Pogorielov [b], Volodymyr Deineka [b], Mykola Lyndin [b], Andrew Rawlinson [c], Ihtesham Ur Rehman [a, *]

[a] *Materials Science and Engineering Department, Kroto Research Institute, University of Sheffield, Sheffield, S3 7HQ, United Kingdom*
[b] *Sumy State University, Medical Institute 31, Sanatornaya st. 40018, Sumy, Ukraine*
[c] *Academic Unit of Restorative Dentistry, School of Clinical Dentistry, University of Sheffield, Sheffield S10 2SZ, United Kingdom*

ARTICLE INFO

ABSTRACT

Tissue engineering approaches have been adapted to reconstruct and restore functionality of impaired tissue for decades. Porous biomimetic composite scaffolds of Chitosan (CH) with hydroxyapatite (HA) for bone regeneration have also been extensively studied in the past. These porous scaffolds play a critical role in providing successful regeneration by acting as a three-dimensional template for delivering nutrients and metabolites and the removal of waste by products. The aim of the current study was to investigate in-*vitro* and in-*vivo* degradation rates of porous freeze gelated chitosan (CH) and CH hydroxyapatite scaffolds by scanning electron microscopy (SEM) to observe for morphological changes, Fourier Transform Infrared Spectroscopy (FTIR) in conjunction with photo-acoustic sampling (PAS) accessory for the analysis of chemical changes, pH analysis and UV–Vis spectroscopy of degraded supernatant. SEM results showed significant alterations in the surface morphology. FTIR-PAS spectra showed changes in the finger print region and glycosidic bonds showed signs of breakage. pH values and UV–Vis spectroscopy of the degraded supernatant were indicative of CH bonds scission in neat samples. HA incorporated specimens showed more stability. Histological sections performed after in-*vivo* implantation also showed greater cellular infiltration and delayed degradation profiles by HA loaded samples. Within 30 days of implantation, neat CH scaffolds showed complete in-*vivo* biodegradation. The current findings show the advantage of adding hydroxyapatite to porous templates which enhances hard tissue regeneration. In addition, it allows easy and cost effective fabrication of bioactive composite scaffolds.

1. Introduction

Tissue engineering approaches have been adapted to reconstruct and restore functionality of impaired tissue for decades. Among these approaches porous scaffolds play a critical role in providing successful regeneration by acting as a three-dimensional (3D) template to carry nutrients/metabolites and promote matrix deposition along with the concomitant removal of waste end products [1]. New fabrication techniques for making polymeric scaffold with 'controlled porosity' that would essentially allow for specific tissue regeneration requirements to be met in a predictable and reproducible manner are adopted in various studies [1,2]. It is well known that there are a number of factors governing scaffold design. The pore architecture should allow efficient cell seeding into the scaffold. In addition it should provide sufficient space for regeneration of newly formed tissue [2]. Most of the studies exploring scaffold synthesis techniques for tissue engineering employ the use of both naturally derived polymers (chitosan, cellulose, silk and gum resins) and synthetic polymers (polyethylene, PVC, silicones and nylon) [3]. Degradation of these polymeric biomaterials used for tissue engineering applications is also a critical factor for successful regeneration of healthy tissue. The rate of degradation should be ideally tailored to be inversely proportional to the rate of new regenerated tissue. The ultimate metabolic fate of an implanted device is an essential aspect that implores

consideration when designing biomaterials with a specific application. The life of an implant device is affected by its ability to uptake and withhold water, which is dependent on the diffusion coefficient of the material. Materials with a high diffusion coefficient bear the tendency to allow water to breach into the matrix allowing water soluble additives to be released more rapidly [4].

Porous biomimetic composite scaffolds of Chitosan (CH) with hydroxyapatite (HA) for bone regeneration have been extensively studied in the past [5–9]. Chitin is the second most abundantly available biopolymer and is used to obtain CH after a series of chemical reactions. CH is an amino polysaccharide, which has attracted significant scientific interest during the past few decades. It is a partially de-acetylated form of chitin, well known for showing biocompatibility, biodegradability and antimicrobial activity [10]. The chemically versatile nature of CH has often placed it at the centre of many investigations conducted by prominent tissue engineering scientists [11]. CH is degraded in-vivo by the action of enzymes, and the degradation rate can be tailored using CH of different molecular weights and degree of deacetylation [10]. Depending on the source and extraction procedures, molecular weights can range from 300 to 1000 kDa. It's pH dependant versatility at low pH (<6) causes amines to be protonated, exhibiting a polycationic nature. At high pH (>6.5) CH amines are deprotonated and reactive, promoting interpolymer associations that encourages fibre, film, porous templates or gel formation [12].

HA [$Ca_{10} (PO_4)_6 (OH)_2$] is a widely used bone substitute, well known to offer a chemical environment that is conductive to new bone formation. It's a calcium phosphate (Ca/P) based bioceramic having a high elastic modulus that undergoes bioresorption when implanted in-vivo. However, it tends to be brittle and is not easily moulded. Due to this property it is used as composite with other polymers. It is now widely used for fabricating biodegradable and stable scaffolds for various tissue engineering applications such as a coating on hip or dental implants. The mechanism of bone resorption by osteoclasts has been extensively studied in the past, whereas studies on resorption of biomaterials surface in-vitro and in-vivo are rarely reported [13–15]. It is assumed that HA resorption occur either by simple dissolution or by cell-mediated process [13].

Scaffolds used for tissue engineering are considered favourable if they have a highly porous structure to support cellular attachment, proliferation and extra cellular matrix (ECM) production [16]. Among the processing techniques available for synthesizing three dimensional (3D) templates such as freeze drying, salt leaching, particulate leaching and lyophilisation, recently freeze gelation has been introduced and has been reported to be a more energy and time efficient method [17]. Phase separation has been employed to synthesize porous scaffolds for tissue engineering applications in the past as well. This technique, achieves phase separation by decreasing the temperature of a polymer solution, resulting in two different phases or gradients, a high polymer concentration and a low polymer concentration (polymer rich and polymer lean phase) [18]. The solvent of the polymer solution is then extracted by evaporation or sublimation to leave behind open pores. The polymer rich part solidifies into the skeleton of the polymer foam. It is usually differentiated in two different types depending on the crystallization temperature of the solvent used in the polymer solution [17,19].

Biodegradation of porous scaffolds aimed at tissue engineering is also a complex phenomenon, the rate of which is dependent on several intrinsic and morphological factors such as pore size, pore morphology, surface area, hydrophilicity and porosity percentage. Recently we have reported the fabrication and characterization of freeze gelated porous scaffolds for use in periodontal regeneration as part of a functionally graded membrane [18]. The aim of the current study was to investigate in-vitro degradation rates of porous freeze gelated CH and CH HA scaffolds by scanning electron microscopy (SEM) to observe for morphological changes, Fourier Transform Infrared Spectroscopy (FTIR) in conjunction with photo acoustic sampling (PAS) accessory for bulk chemical changes, pH analysis and UV–Vis spectroscopy of degraded supernatant and Histological sections after in-vivo implantation. It is envisaged that insight into these parameters will guide us in further tuning/tailoring of porous scaffolds.

2. Materials and methods

Chitosan (0.9 gm) having medium molecular weight (75–85% Deacetylated, 190–310 kDa) was dissolved in 0.2 M L-Ascorbic acid (ASa) (99.9%, Sigma Aldrich, UK) or Acetic acid (Anal R Grade, Fisher Scientific. UK) to create 3% wt/v solutions with or/and without HA. This solution was kept stirring for 6 h (hr) before adding HA (0.9 gm). Medical grade HA (Captal S™, Plasma Biotal Limited, UK), was incorporated in a ratio of 50:50. After addition of HA, solutions were stirred for 12 h at room temperature and then cast into a petri dish before storing at 4 °C for 3 h and then at −20 °C for 12 h. A pre-cooled solution of Sodium hydroxide 3 M in 100% ethanol in a ratio of 1:1 (v/v) was used to submerge frozen membranes for 12 h. Membranes were then washed with phosphate buffered saline (PBS) to elude the remaining neutralizing solution and specimens were dried using a series of ethanol washes for 15 min each. After this the samples were immersed in a solution of glycerol (Fisher Scientific. UK) and distilled water in a ratio of 1:10 for 15 min and removed to air dry and stored at room temperature [18]. In total four different membranes were fabricated, denoted as ASa-CH, ASa-CH:HA, ACa-CH and ACa-CH:HA. At each time point samples were assessed with SEM, FTIR, pH and UV–Vis spectroscopy.

2.1. Scanning electron microscopy (SEM)

SEM was performed to study the surface and cross-sectional morphology of FG membranes (spot size: 3.0, voltage range 5–10 kV, Philips X-L 20 microscope). Samples were mounted on aluminium stubs with double-sided carbon adhesive dots and were sputter coated under vacuum with carbon using Speedivac carbon coating unit (Model 12E6/1598).

2.2. pH analysis

pH measurements of the supernatant were performed on Mettler Toledo S20 Seven Easy pH meter at each time point by first calibrating the pH meter in standard solutions and then immersing the bulb until the reading stabilized.

2.3. UV–Vis spectroscopy

Ultra violet visible spectrophotometry was performed on LAMBDA 950 UV Vis spectrophotometer (PerkinElmer) by taking blank background and Phosphate buffered saline (PBS) was used as a reference. Analysis was performed between ranges of 200–500 nm. A quartz cell (Thor Labs Inc. UK) was used to record the UV–Vis reading.

2.4. In-vivo study

In-vivo studies were performed to assess the cellular and degradation response of FG membranes after implantation. Experiments were conducted at the Medical Institute of Sumy State University and were approved by the Institutional Commission on Biomedical Ethics (#16/12 on 15/12/2014). 48 chinchilla rabbits,

aged 8–9 months, were used in the experiment. Animals were housed at 22 ± 2 °C on a 12 h light/dark cycle and received food and water "ad libra". Keeping of the animals and experiments were carried in accordance with the Directive 2010/63/EU of the European Parliament and of the Council of 22 September 2010 on the Protection of Animals Used for Scientific Purposes and The General Ethical Principles for Experiments on Animals, which were accepted by the First Bioethics National Congress (Kyiv, 2001).

All animals were divided into four groups according to the materials that were used for implantation;

1 group 1–Chitosan in acetic acid (ACa-CH)
2 group 2–Chitosan in acetic acid with 50:50 Hydroxyapatite (ACa-CH:HA)
3 group 3–Chitosan in ascorbic acid (ASa-CH)
4 group 4–Chitosan in ascorbic acid with 50:50 Hydroxyapatite (ASa-CH:HA)

2.5. Operation design

After administration of general anesthesia (Ketamine 7 mg/kg and thiopental 10 mg/kg) and peripheral vein catheterization, the left thigh was shaved to prepare the implantation site. The surgical site was treated with C-4 solution, a longitudinal incision was made on lateral surface of the thigh and muscles were separated to gain access to the bone. A round bone defect was made up to the bone marrow using a 10 mm drill. The defect was filled by the grafts that had similar dimensions in diameter and did not need fixation. All the grafts were sterilized in 96% ethanol for 1hr prior to implantation. After completion of the implantation procedure the wound was sutured and as a prophylaxis of postoperative bacterial complications animals were given antibiotic (ceftriaxone, 50 mg per 1 kg) for 1 week. The animals were killed at 7 and 30 days after the operation (narcosis overdose - ketamine, 70 mg/kg).

2.6. Histology

After the animals were sacrificed; the grafts were removed with some surrounding bone to prevent any damage to the graft. All samples were fixed in 10% formaldehyde for 24 h and decalcified in 4.5% of acetic acid for 48 h. The sample were then dried in alcohol solutions of elevated concentrations and set into paraffin wax. 12–15 μm histological sections were prepared and stained with hematoxylin and eosin. The specimens were analyzed for morphometric analysis using a light microscope "OLYMPUS" with SEO Image Lab Bio software (Sumy, Ukraine, license number 27335). From each sample, 10 histological slides were prepared, out of which 5 slides were prepared from the deep zone and 5 slides from the superficial zone respectively. Each slide was divided into 6 zones. Measurements were then done in such a way that the square of empty pores, fibrous tissue and osteoid filled pores in each from 6 zones. The percentage of these parameters was then calculated from each slide of every sample. Cells and fibroblast density was calculated per 1 mm^2 in each slide and calculated for the entire sample in total. Statistical analysis was performed using SPSS software (version 21.1) and data was expressed as mean ± SEM. Statistical significance was defined as $p \leq 0.05$.

3. Results and discussion

A biomimetic multi tiered scaffold that undergoes degradation within a stipulated time frame (with release of bio inert by products) is crucial for allowing the targeted damaged periodontal tissues to undergo complete and uninterrupted regeneration of cellular hierarchical architecture and the extracellular matrix. Moreover, this inevitably circmuvents the tedious and locally tissue destructive practice of performing a secondary stage surgical intervention for retrieval of the template after it has performed the task of tissue rehabilitation and support. For the secondary procedure would surely present a credible threat to the integrity of the newly regenerated sub structures and the re established micro environment. Degradation of CH is known to take place via hydrolysis, as interactions with water molecules breaks the polymeric network into smaller chains whereby the β-1-4 N-acetyl glucosamine units of CH undergo chain scission mainly by lysozymes present in the body. This phenomenon leads to release of amino sugars, which can be incorporated into metabolic pathways or excreted through the body [11,20–22]. Other by products of CH degradation include saccharides which become part of the normal metabolic process [23]. Peter et al., and Mota et al., reported that the addition of Bioglass™ to CH reduced the degradation rate, and attributed this to a decrease in weight loss to the neutralization of the acidic products of CH by the alkali groups [24–26]. To our knowledge this is the first report about detailed degradation characteristics of porous chitosan hydroxyapatite fabricated via freeze gelation.

3.1. Scanning electron microscopy (SEM)

SEM of neat freeze gelated samples has been reported earlier by us [18]. After degradation (Fig. 1a–h) of 21 days in immersion in lysozyme solution, drastic topographical changes in the surface and cross sectional morphology were observed. It appears that surface of ACa-CH and ASa CH displayed relatively higher levels of erosion when compared with ASa-CHHA. No visible pores could be seen. Cross-sectional images of all samples showed eroded edges of the pores in some places. The pore boundary was irregular with signs of breakdown in the continuity of the edges. Somewhat greater surface alterations were also noticed on neat ASa-CH and ACa CH scaffold after 21 days. A study conducted by She and co-workers on the degradation characteristics of porous CH scaffolds have reported similar alterations in the topographical and morphological features after lysozyme treatment. Moreover, they mentioned that after 6 weeks of degradation, the number and size of pores decreased and a sheet like structure appeared on the pores [27]. This is similar to results observed in the current study as pores become denuded.

3.2. pH analysis

Alterations in the pH value were observed after degradation. These values were monitored over the experimental time point shown in Fig. 2. All scaffolds followed a trend of gradual increment of pH with time. pH of degradation media was 6.9 at Day 0 and increased to 8.4 at 48th day. ASa-CH samples showed a spike in the pH to 7.5 at day 14, which showed an increasing trend till day 48. Change in the pH values is more prominent from Day 21–48. Wound healing has been regarded as a complicated regeneration process, which is comprised of intercalating degradation and reassembly of connective tissue. The pH value has a direct and indirect relationship in all biochemical reactions occurring in the process of regeneration. It has been speculated that a low pH is favourable for healing in certain scenarios. Schneider et al., conducted a detailed analysis on the effect of pH on wound healing and concluded that the final pH around a wound is a potent influential factor for the final result of any therapeutics intervention. They also reported that chronic wounds are characterized with high bacterial colonies, that have a local pH of around 7.3 and an acidic environment tends to promote the healing process [28]. With respect to
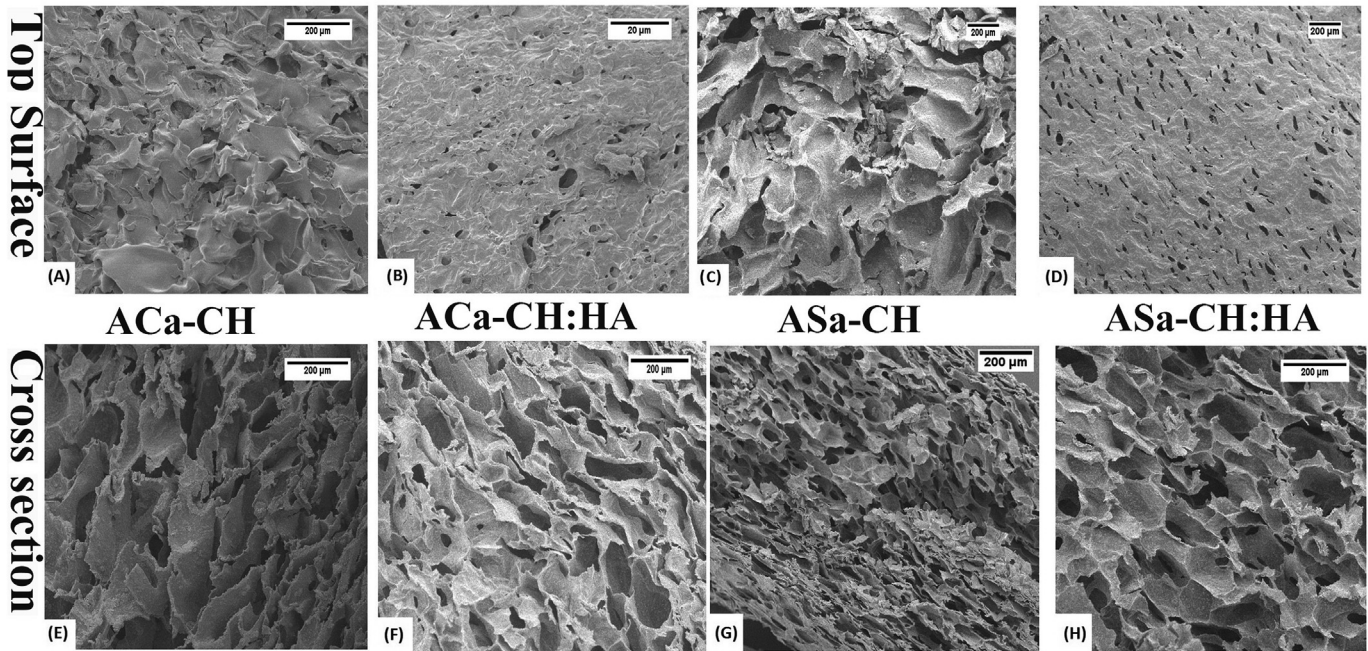
Fig. 1. After degradation of 21 days, SEM micrographs of porous freeze gelated chitosan Top surface of (a) ACa-CH, (b)ACa-CH:HA, (c)ASa-CH and (d) ASa-CH:HA and Cross sectional image of (e) ACa-CH, (f)ACa-CH:HA, (g)ASa-CH and (h) ASa-CH:HA. All images scaled at 200 μm.

the results in the current study, final pH values after degradtion of CH changed from 6.9 to 8.4. However, these are in-*vitro* results which can vary when performed in-*vivo* conditions. Another study reported an increase in the pH profile of pure CH scaffolds, which are similar to the findings obtained in this study. Wan and co-workers noticed that the magnitude of change was insignificantly altered over the incubation period [29]. The change in pH observed in our studies could be attributed to the release of −NH$_2$ groups at the C-2 position as a result of bond cleavage in the lysozyme solution. Some of these ions in turn may form complexes with OH ions thereby increasing the pH as the degradtion proceeds [30].

3.3. UV−Vis spectroscopy

UV−Vis spectroscopy performed on the degraded media of freeze gelated scaffolds is shown in Fig. 3. Degradation of CH is known to give rise to two new absorption bands at 230 and 290 nm which are correlated with carboxylic acid and aldehyde group occurring after oxidative scission of glycosidic bonds. These two bands vary in intensity over the degradation period visible by the alterations in the intensities (Fig. 3 e and f). UV−Vis spectroscopy of

pH Change of Degraded Membranes

Fig. 2. pH analysis of degraded supernatant over a period of 28 days of degradation. pH was taken at each time point. Values shown are mean ± SEM (n = 3).

degraded freeze gelated scaffolds (Fig. 3 a to d) showed prominent bands observed in the range of 200−300 nm which point towards hydrolytic scission of β, 1−4 glycosidic bonds of CH. Plain CH is known to exhibit a strong absorption band at 200, which is visible in all spectra. A band at 230 nm may appear due to *n*-σ*(nonbonding to antibonding) transition of amino groups and π-π* transition of carbonyl and carboxyl groups. The second band at 290 nm was ascribed to n- π* transition of carbonyl or carboxyl groups. These bands are indicative of bond breakage or molecular bonds moving from bonding to anti-bonding. A study performed by El-Sawy et al., previously reported similar findings [31]. Ulanski and co-workers conducted a study on the radiation induced changes in CH and reported that the appearance and upward curvature of the bands is due to carbon oxygen double bonds occurring after the bond breakage of CH and −H abstraction reaction which is followed by ring opening [32]. Another study conducted by Czechowska et al., reported that CH bands appear at 265 and 297 nm, which they also designated to carbonyl groups. The increased intensity of these bands with time was ascribed to increasing efficiency of −OH re-action with CH on reduction of molecular weight. It could also be indicative of partial formation of carbonyl groups [33].

Optical images of the scaffolds taken at different time points to see visual changes in macro structure are shown in Fig. 4. From Day 1−54, ACa-CH showed rapid breakdown in the size of the specimen as compared to other scaffolds. This is visible at day 14. At day 21 the rest of the specimens also showed signs of cracks. ASa-CH showed stability after being subjected to lysozyme media. ACa-CHHA also shows firmness till day, 14 which is similar to images of ASa-CHHA.

3.4. H& E sections after in-vivo implantation

Examination of the histology slides showed a population of cells that was heterogeneous. The cellular morphologies thus observed were consistent with osteoblasts, osteocytes and fibroblasts in some regions as detailed below.
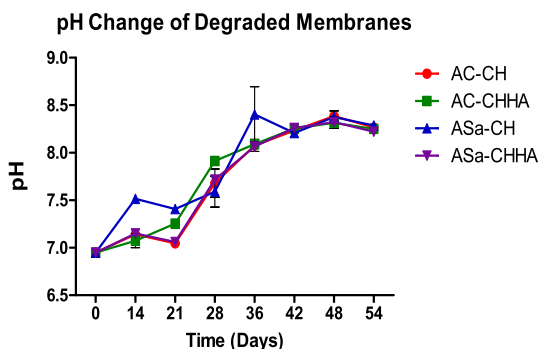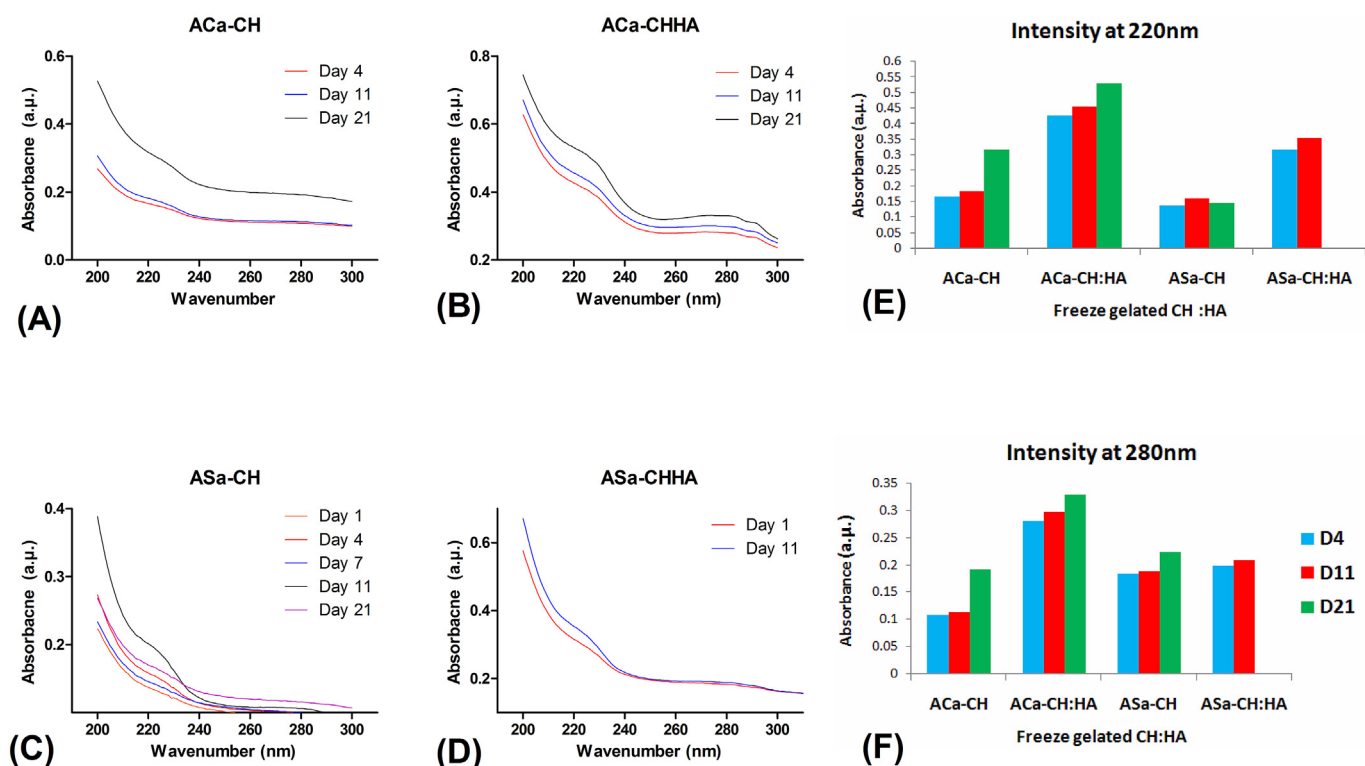
Fig. 3. UV Vis spectral data of degraded media of freeze gelated scaffolds (a) ACa-CH, (b) ACa-CHHA, (c) ASa-CH, (d) ASa-CHHA, samples were analyzed in a quartz cell depending on the availability of degraded solution obtained at different time point, (e and f), Images show intensity plotted against absorbance at 280 and 220 nm.

3.4.1. First harvest point (7 days)

All animals were alive and anesthetized when grafts were placed inside the implantation site. No macroscopic reaction was observed at the implantation site. H & E images (Figs. 5 and 6) showed difference in between CH and CH:HA samples. All microscopic examinations showed the bony defect was filled with implanted amorphous material and degenerated cells. In pure CH membrane grafts, two zones could be distinguished; 1) superficial zone, the part of implant in contact with bone and bone marrow, and 2) deep zone (Fig. 5 a, b, c and d). Images obtained from the deep zone were void of cells. Pores that were located near bone were filled with newly formed bone tissue (Fig. 5 c and d).

HA loaded samples (Fig. 6 e, f, g and h) showed higher numbers of cellular infiltration as compared to neat CH membranes. Observation of the zone close to bone in HA loaded samples revealed less empty pores. Cellular infiltration of ASa-CH:HA samples was higher as compared to ACa-CH:HA. Cells could be seen accumulating on top of one another in a layer by layer manner with in the porosities of the scaffold in Fig. 5 e and f. Larger and somewhat empty pores can be appreciated in Fig. 5 a and b, on neat CH samples as compared to CH HA membranes. Deeper zone facing the bone also showed cellular accumulation in Fig. 5 c and d.

3.4.2. Second harvest point

At the end of second time point on visual inspection some evidence of periosteal reaction was noted after the bone removal from all specimens. This was noted as a small elevation of bone over the implantation site. No colour difference was seen at this site, hence, this was taken to be indicative of new bone formation on implant site. No difference was seen in between neat freeze gelated CH and HA loaded specimens at this stage.

Histological, H and E images taken on the 30th day showed significant bone in-growth when compared with first time-point

after 7th day of implantation. Neat CH membranes completely degraded till 30th day (Fig. 6 a and b) after the operation and no signs of remnants of the specimen were observed. Bone defects are filled with usually three types of tissues — bone, fibrous tissue and bone marrow. Bone tissue that occupied the most peripheral part of the defect formed a trabecular network. Osteoblasts lie on the trabecular surface, while osteocytes lie in lacunae (these can be observed on the inside of trabeculae). The thickness of the trabecular part decreased from the peripheral to central zone of the defect. Inter-trabecular spaces fill with bone marrow cells that migrate from the non-injured parts of the bone. In the central part of the defect, fibrous tissue was observed that was tightly connected with new bone tissue and will probably be replaced in at a later stage. Also, fibrous tissue could be found within inter-trabecular spaces, especially in central zone of defect. Morphometric parameters did not show significant difference in between ASa-CH and ACa-CH scaffolds (Table 1). However, significantly more osteoblasts were noted in HA loaded groups. The number of pores in ASa-CH:HA and ACa-CH:HA scaffolds is reduced by 30 and 35% respectively; in contrast to the neat CH implanted scaffolds. This is indicative of migration of osteoblasts and subsequent colonization of the pores with secretion of bone matrix. Osteoid formation noted in our ACa-CH: HA and ASa-CH:HA loaded samples at 13.7 and 12.9% respectively by day 7 (Table 1), is an encouraging sign hinting towards future mineralization of the bone matrix. Osteoblasts persisted at relatively higher levels at the defect sites that received the HA loaded samples as compared to the neat samples by day 30 (Table 2). This indicates an active phase of osteoblasts geared towards bone matrix deposition and maturation. HA can stimulate bone cells migration. Thus its incorporation into our scaffolds leads to presence of a significant increment of osteoblasts in the early stage of bone formation. Moreover, no significant differences were noted in the number of osteocytes for neat
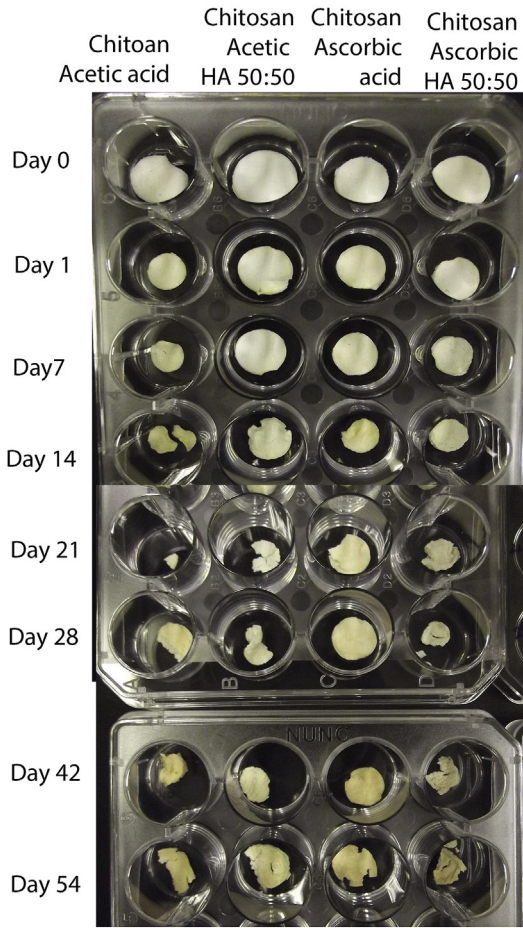
Fig. 4. Optical Images taken from a DSLR Nikon Camera of scaffolds at different time points after drying and subjected to degradation media till 54 days.

the operation that is indicative of the tissue maturation within the defect site. Fibrous tissue presents in all specimens except ASa-CH and ACa-CH, as compared to HA loaded samples which had three times more fibrous tissue. ASa-CH and ACa-CH groups were completely replaced by new tissue while there is $3.9 \pm 0.7\%$ and $4.3 \pm 0.5\%$ of template remnants of ASa-CH:HA and ACa-CH:HA groups (Table 2). This could be due to HA, that decreased the overall degradation rate of CH based scaffolds. The aim of the in-vivo studies was to look into the effect of cellular infiltration and degradation behaviour of freeze gelated CH:HA membranes. The evaluation of bone TE templates in an in-vivo condition is usually a positive step towards the clinical setting after drawing encouraging inferences from detailed in-vitro characterizations and analyses [34]. In-vivo studies conducted on porous CH:HA scaffolds reported in the past have mentioned that composite scaffolds are able to support more bone as compared to neat CH scaffolds [34–37]. Jin and co-workers reported that after in-vivo implantation in mice, composite scaffolds provided a strong effect on bone formation. More pronounced features of newly formed bone tissue were prominent after the 8 weeks of implantation. This is in spite of the findings put forth by Danilchenko et al., reported that after 10 days of implantation, intense biodegradation is triggered and newly formed tissue completely replaces the CH:HA composite on the 24th day of implantation [35]. Furthermore, they also mentioned that the newly formed tissue had not only osteoblasts, but also osteoclasts and Howship's Lacunae present within its structure [36]. In the current study, histological images and morphometric data results (Tables 1 and 2) from the first time point (Fig. 5 a to h) were suggestive of CH:HA membranes as favourable for cellular infiltration and subsequent secretion of ECM. To that end, our findings are in agreement with previous studies [35,36]. Break-down of HA is known to occur through the resorption process [38]. HA seems to have a significant effect when it comes to increasing cellular infiltration within the first 7 days of implantation. At the second time point, HA incorporated scaffolds did not display complete degradation (Fig. 6). In the central zone of the defect their remnants can be observed, in both ACa-CH:HA and ASa-CH:HA. When compared with the neat CH:FG scaffolds, defect zone were filled mostly by bone tissue and bone marrow cells. Some images were also suggestive of fibrous tissue. Bone trabeculae had similar

and HA loaded groups. Fibroblasts were present in all series but their number was significantly less in apatite loaded groups. In general, the cell density decreases compared to the 7th day after
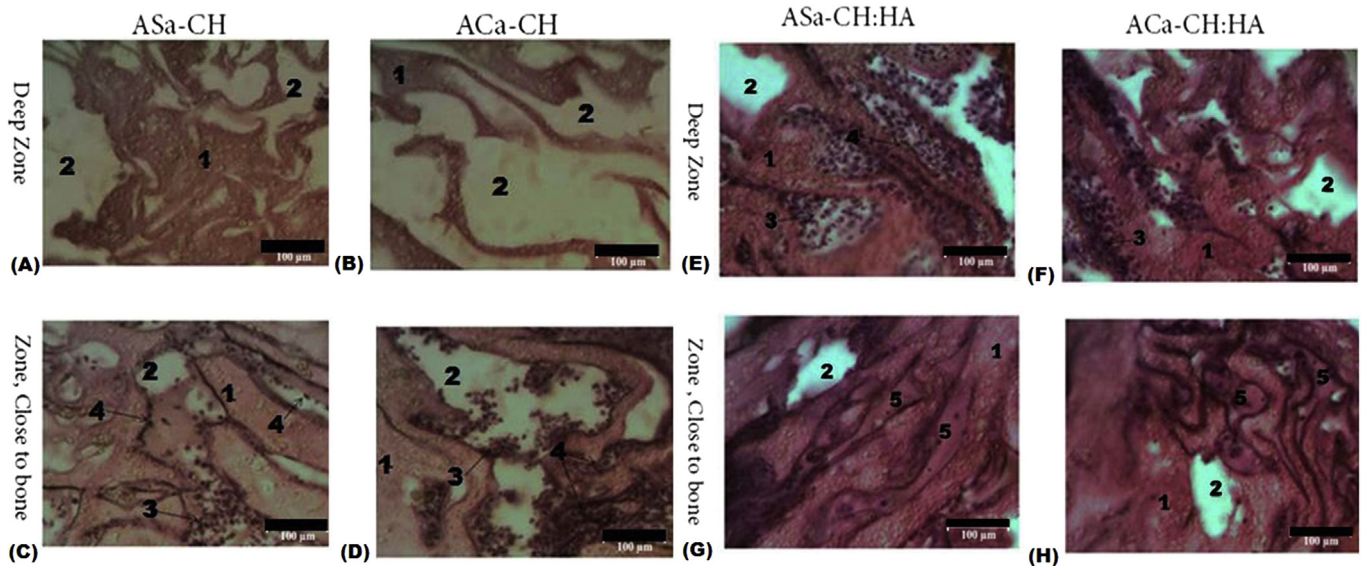
Fig. 5. H & E staining performed on deep zones (a) ASa-CH (b) ACa-CH, Zone close to bone are shown as (c) ASa-CH and (d) ACa-CH, deep zones (e) ASa-CHHA (f) ACa-CHHA Zone close to bone are shown as (g) ASa-CH:HA and (h) ACa-CH:HA. Zones closer to bone show more cellular infiltration within the pores and ACa-CH show more cells than ASa-CH, Images were taken at 7 days after bone implantation, magnification 300×: 1–CH; 2–empty pore; 3–leukocyte; 4–fibroblast; 5–osteoid. All images scaled at 100 μm.
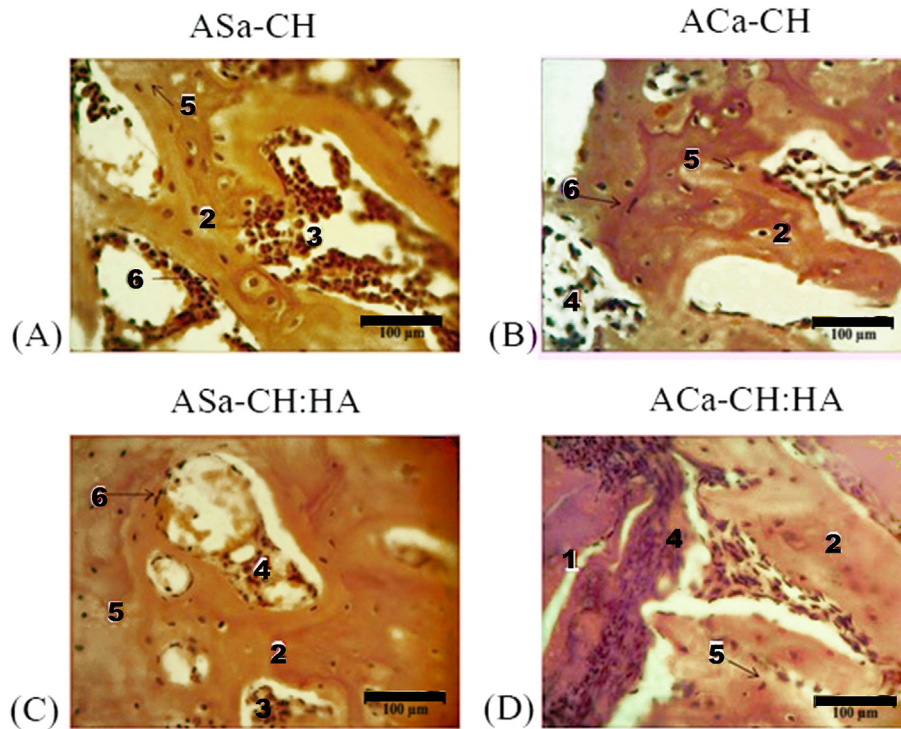
Fig. 6. H & E histological image of CH FG membranes at day 30 after bone implantation, magnification 300×:1—remnant of CH scaffold, 2—bone trabeculae, 3—bone marrow, 4—fibrous tissue, 5—osteocyte, 6—osteoblast, All images scaled at 100 μm.

Table 1
Morphometric parameters of CH scaffolds in 7 days after bone implantation. Empty pores, fibrous and osteoid tissue - % from slide surface, cell density and fibroblast — number per 1 mm^2.

	ASa-CH	ASa-CH:HA	ACa-CH	ACa-CH:HA
Empty pores	58.6 ± 2.6	42.5 ± 3.1 p = 0.002	54.1 ± 1.8	38.6 ± 2.3 p = 0.0003
Fibrous tissue	24.8 ± 1.6	21.7 ± 0.9 p = 0.12	22.3 ± 1.2	19.4 ± 1.4 p = 0.14
Osteoid	—	12.9	—	13.7
Cell density	23.5 ± 1.2	45.2 ± 3.7 p = 0.0002	19.8 ± 2.5	39.6 ± 4.1 p = 0.002
Fibroblast	4.6 ± 0.4	11.6 ± 0.8 p = 0.0001	3.9 ± 0.5	13.3 ± 1.2 p = 0.0001

thickness in peripheral and central zones of defects. It is suggested that HA stimulated bone in-growth in all part of defects, and as reported by previous groups, trabeculae were covered with osteoblasts, that had higher density. As HA addition is known to have a

Table 2
Morphometric parameters of CH scaffolds in 30 days after bone implantation. Bone, fibrous tissue and remnant of scaffold - % from slide surface, osteoblast, osteocyte and fibroblast — number per 1 mm^2.

	ASa-CH	ASa-CH:HA	ACa-CH	ACa-CH:HA
Bone tissue	35.6 ± 2.8	49.2 ± 1.4 p = 0.001	31.8 ± 1.9	46.3 ± 4.2 p = 0.01
Fibrous tissue	11.5 ± 1.3	3.9 ± 0.7 p = 0.0004	9.4 ± 0.9	4.3 ± 0.5 p = 0.0006
Remnant of scaffold	—	5.9 ± 0.3	—	3.5 ± 0.4
Osteoblast	16.5 ± 1.2	27.4 ± 1.6 p = 0.0003	19.3 ± 2.1	31.9 ± 4.2 p = 0.02
Osteocyte	4.3 ± 0.8	3.7 ± 0.5 p = 0.53	5.7 ± 0.8	4.6 ± 0.4 p = 0.45
Fibroblast	5.3 ± 0.5	2.8 ± 0.4 p = 0.002	4.8 ± 0.3	3.2 ± 0.7 p = 0.06

stimulatory effect on cell migration and osteoblastic activity, it is probably a key factor for bone ingrowth. In another study conducted by Chesnutt and co-workers, it was reported that CH nano-HA scaffolds induce osteocalcin production by osteoblasts in-*vitro* and support bone formation in-*vivo* [37].

4. Conclusion

The current investigation revolves around the significance of hydroxyapatite incorporation in porous freeze gelated chitosan scaffolds using acetic acid and ascorbic acid as solvents, and how this would influence in-vitro and in-vivo degradation rates of the designed templates. Freeze gelated samples with hydroxyapatite showed decreased susceptibility to lysozyme degradation as shown by optical images taken at each time points over the 54 days degradation period, and spectroscopic studies performed by FTIR-PAS showed neat chitosan specimens were also somewhat stable over the experimental period. Histological sections performed after *in-vivo* implantation also showed greater cellular infiltration and delayed degradation by HA loaded samples. Within the 30 days of implantation, neat chitosan scaffolds showed complete biodegradation in *in-vivo* conditions. The current findings show the advantage of adding hydroxyapatite to porous templates aimed at regenerating hard tissue. The evidence thus presented in this study clearly demonstrates their immense potential for use in fabricating composite templates aimed at bone tissue engineering applications in the clinical setting.

Appendix A. Supplementary data

Supplementary data related to this article can be found at http://dx.doi.org/10.1016/j.polymdegradstab.2016.11.018.

References

[1] S.J. Hollister, Porous scaffold design for tissue engineering, Nat. Mater 4 (2005) 518—524.

[2] D. Yoo, New paradigms in hierarchical porous scaffold design for tissue engineering, Mater Sci. Eng. C Mater Biol. Appl. 33 (2013) 1759—1772.

[3] Y. Wan, A. Yu, H. Wu, Z. Wang, D. Wen, Porous-conductive chitosan scaffolds for tissue engineering II. in vitro and in vivo degradation, J. Mater Sci. Mater Med. 16 (2005) 1017—1028.

[4] V.M. Correlo, E.D. Pinho, I. Pashkuleva, M. Bhattacharya, N.M. Neves, R.L. Reis, Water absorption and degradation characteristics of chitosan-based polyesters and hydroxyapatite composites, Macromol. Biosci. 7 (2007) 354—363.

[5] X. Cai, L. Chen, T. Jiang, X.Y. Shen, J.M. Hu, H. Tong, Facile synthesis of anisotropic porous chitosan/hydroxyapatite scaffolds for bone tissue engineering, J. Mater Chem. 21 (2011) 12015—12025.

[6] X. Cai, H. Tong, X. Shen, W. Chen, J. Yan, J. Hu, Preparation and characterization of homogeneous chitosan—polylactic acid/hydroxyapatite nanocomposite for bone tissue engineering and evaluation of its mechanical properties, Acta Biomater. 5 (2009) 2693—2703.

[7] N. Maganti, P.K.C. Venkat Surya, W.W. Thein-Han, T.C. Pesacreta, R.D.K. Misra, Structure—process—property relationship of biomimetic chitosan-based nanocomposite scaffolds for tissue engineering: biological, physico-chemical, and mechanical functions, Adv. Eng. Mater 13 (2011) B108—B122.

[8] N. Siddiqui, K. Pramanik, Effects of micro and nano β-TCP fillers in freeze-gelled chitosan scaffolds for bone tissue engineering, J. App Polym. Sci. 131 (2014).

[9] W.W. Thein-Han, R.D.K. Misra, Biomimetic chitosan—nanohydroxyapatite composite scaffolds for bone tissue engineering, Acta Biomater. 5 (2009) 1182—1197.

[10] C. Cunha-Reis, K. TuzlaKoglu, E. Baas, Y. Yang, A. El Haj, R.L. Reis, Influence of porosity and fibre diameter on the degradation of chitosan fibre-mesh scaffolds and cell adhesion, J. Mater Sci-Mater Med. 18 (2007) 195—200.

[11] T. Kean, M. Thanou, Biodegradation, biodistribution and toxicity of chitosan, Adv. Drug Del Rev. 62 (2010) 3—11.

[12] H. Yi, L.Q. Wu, W.E. Bentley, R. Ghodssi, G.W. Rubloff, J.N. Culver, et al., Biofabrication with chitosan, Biomacromol 6 (2005) 2881—2894.

[13] T. Goto, T. Kojima, T. Iijima, S. Yokokura, H. Kawano, A. Yamamoto, et al., Resorption of synthetic porous hydroxyapatite and replacement by newly formed bone, J. Orthop. Sci. 6 (2001) 444—447.

[14] S. Wenisch, J.P. Stahl, U. Horas, C. Heiss, O. Kilian, K. Trinkaus, et al., In vivo mechanisms of hydroxyapatite ceramic degradation by osteoclasts: fine structural microscopy, J. Biomed. Mater Res. Part A 67A (2003) 713—718.

[15] E. Rumpel, E. Wolf, E. Kauschke, V. Bienengraber, T. Bayerlein, T. Gedrange, et al., The biodegradation of hydroxyapatite bone graft substitutes in vivo, Folia Morphol. (Warsz) 65 (2006) 43—48.

[16] T.B.F. Woodfield, J. Malda, J. de Wijn, F. Peters, J. Riesle, C.A. van Blitterswijk, Design of porous scaffolds for cartilage tissue engineering using a three-dimensional fiber-deposition technique, Biomaterials 25 (2004) 4149—4161.

[17] M.-H. Ho, P.-Y. Kuo, H.-J. Hsieh, T.-Y. Hsien, L.-T. Hou, J.-Y. Lai, et al., Preparation of porous scaffolds by using freeze-extraction and freeze-gelation methods, Biomaterials 25 (2004) 129—138.

[18] S.B. Qasim, R.M. Delaine-Smith, T. Fey, A. Rawlinson, I.U. Rehman, Freeze gelated porous membranes for periodontal tissue regeneration, Acta Biomater. 23 (2015) 317—328.

[19] H. Liu, J. Mao, K. Yao, G. Yang, L. Cui, Y. Cao, A study on a chitosan-gelatin-hyaluronic acid scaffold as artificial skin in vitro and its tissue engineering applications, J. Biomater. Sci. Polym. Ed. 15 (2004) 25—40.

[20] K. Tomihata, Y. Ikada, In vitro and in vivo degradation of films of chitin and its deacetylated derivatives, Biomaterials 18 (1997) 567—575.

[21] D. Ren, H. Yi, W. Wang, X. Ma, The enzymatic degradation and swelling properties of chitosan matrices with different degrees of N-acetylation, Carbohydr. Res. 340 (2005) 2403—2410.

[22] Y.G. Liu, C.R. Zhou, Y. Sun, A biomimetic strategy for controllable degradation of chitosan scaffolds, J. Mater Res. 27 (2012) 1859—1868.

[23] M.N.V.R. Kumar, R.A.A. Muzzarelli, C. Muzzarelli, H. Sashiwa, A.J. Domb, Chitosan chemistry and pharmaceutical perspectives, Cheml Rev. 104 (2004) 6017—6084.

[24] J. Mota, N. Yu, S.G. Caridade, G.M. Luz, M.E. Gomes, R.L. Reis, et al., Chitosan/bioactive glass nanoparticle composite membranes for periodontal regeneration, Acta Biomater. 8 (2012) 4173—4180.

[25] X. Li, K. Nan, S. Shi, H. Chen, Preparation and characterization of nano-hydroxyapatite/chitosan cross-linking composite membrane intended for tissue engineering, Int. J. Biol. Macromol. 50 (2012) 43—49.

[26] M. Peter, N.S. Binulal, S. Soumya, S.V. Nair, T. Furuike, H. Tamura, et al., Nanocomposite scaffolds of bioactive glass ceramic nanoparticles disseminated chitosan matrix for tissue engineering applications, Carbohyd Polym. 79 (2010) 284—289.

[27] Z.D. She, B.F. Zhang, C.R. Jin, Q.L. Feng, Y.X. Xu, Preparation and in vitro degradation of porous three-dimensional silk fibroin/chitosan scaffold, Polym. Degrad. Stab. 93 (2008) 1316—1322.

[28] L.A. Schneider, A. Korber, S. Grabbe, J. Dissemond, Influence of pH on wound-healing: a new perspective for wound-therapy? Arch. Dermatol Res. 298 (2007) 413—420.

[29] Y. Wan, H. Wu, X.Y. Cao, S. Dalai, Compressive mechanical properties and biodegradability of porous poly(caprolactone)/chitosan scaffolds, Polym. Degrad. Stab. 93 (2008) 1736—1741.

[30] M. Rinaudo, Chitin and chitosan: properties and applications, Prog. Polym. Sci. 31 (2006) 603—632.

[31] N.M. El-Sawy, H.A. Abd El-Rehim, A.M. Elbarbary, E.S.A. Hegazy, Radiation-induced degradation of chitosan for possible use as a growth promoter in agricultural purposes, Carbohyd Polym. 79 (2010) 555—562.

[32] P. Ulanski, J. Rosiak, Preliminary studies on radiation-induced changes in chitosan, Rad. Phys. Chem. 39 (1992) 53—57.

[33] R. Czechowska-Biskup, B. Rokita, S. Lotfy, P. Ulanski, J.M. Rosiak, Degradation of chitosan and starch by 360-kHz ultrasound, Carbohyd Polym. 60 (2005) 175—184.

[34] A.M. Martins, J.D. Kretlow, A.R. Costa-Pinto, P.B. Malafaya, E.M. Fernandes, N.M. Neves, et al., Gradual pore formation in natural origin scaffolds throughout subcutaneous implantation, J. Biomed. Mater Res. A 100 (2012) 599—612.

[35] S.N. Danilchenko, O.V. Kalinkevich, M.V. Pogorelov, A.N. Kalinkevich, A.M. Sklyar, T.G. Kalinichenko, et al., Characterization and in vivo evaluation of chitosan-hydroxyapatite bone scaffolds made by one step coprecipitation method, J. Biomed. Mater Res. Part A 96A (2011) 639—647.

[36] H.H. Jin, D.H. Kim, T.W. Kim, K.K. Shin, J.S. Jung, H.C. Park, et al., In vivo evaluation of porous hydroxyapatite/chitosan-alginate composite scaffolds for bone tissue engineering, Int. J. Biol. Macromol. 51 (2012) 1079—1085.

[37] B.M. Chesnutt, Y. Yuan, K. Buddington, W.O. Haggard, J.D. Bumgardner, Composite chitosan/nano-hydroxyapatite scaffolds induce osteocalcin production by osteoblasts in vitro and support bone formation in vivo, Tissue Eng. Part A 15 (2009) 2571—2579.

[38] Y. Shikinami, Y. Matsusue, T. Nakamura, The complete process of bio-resorption and bone replacement using devices made of forged composites of raw hydroxyapatite particles/poly L-lactide (F-u-HA/PLLA), Biomaterials 26 (2005) 5542—5551.